Earthquakes and Structures, Vol. 3, No. 6 (2012) 869-887
DOI: http://dx.doi.org/10.12989/eas.2012.3.6.869

Effects of ground motion scaling on nonlinear higher mode building response

R.L. Wood and T.C. Hutchinson*

Department of Structural Engineering, University of California, San Diego, La Jolla, CA, USA

(Received April 13, 2011, Revised June 18, 2012, Accepted July 3, 2012)

Abstract. Ground motion scaling techniques are actively debated in the earthquake engineering community. Considerations such as what amplitude, over what period range and to what target spectrum are amongst the questions of practical importance. In this paper, the effect of various ground motion scaling approaches are explored using three reinforced concrete prototypical building models of 8, 12 and 20 stories designed to respond nonlinearly under a design level earthquake event in the seismically active Southern California region. Twenty-one recorded earthquake motions are selected using a probabilistic seismic hazard analysis and subsequently scaled using four different strategies. These motions are subsequently compared to spectrally compatible motions. The nonlinear response of a planar frame-idealized building is evaluated in terms of plasticity distribution, floor level acceleration and uncorrelated acceleration amplification ratio distributions; and interstory drift distributions. The most pronounced response variability observed in association with the scaling method is the extent of higher mode participation in the nonlinear demands.

Keywords: earthquake engineering; nonlinear analysis; ground motion scaling; geometric mean; spectrally compatible; structural engineering

1. Introduction

Given the broad nature of earthquake motions, coupled with limited resources to analyze a particular problem, a natural question that arises in design is: How should a suite of motions be scaled to reasonably represent the anticipated seismic hazard at the site where it will be constructed? Previous ground motion scaling methods have primarily focused on spectral acceleration amplitude scaling based, often at the fundamental period of the structure (T_1) (e.g. Shome and Cornell 1998). Although appealing, this scaling method only focuses on the first-mode linear response of the structural building system. Buildings designed to respond nonlinearly, with anticipated soil-structure-interaction, or if one is concerned with secondary system response (nonstructural component systems), scaling at periods other than the fundamental mode are of interest. As a result, it may also be desirable to scale the motion across a period range in which the structure is anticipated to vibrate during seismic excitation. ASCE 7-05 (2006) recognizes these issues by requiring that the average spectral acceleration of the suite of motions used for nonlinear time history analyses be greater than or equal to the target spectral acceleration over the range of $0.2T_1$ to $1.5T_1 s$. In the design codes, it is required to match or exceed the target spectrum over the range of periods to evaluate structures

*Corresponding author, Professor, E-mail: tahutchinson@ucsd.edu

which are anticipated to respond nonlinearly and contain responses contributed by higher modes. The upper bound of the scaling range, $1.5T_1$, is associated with the period elongation due to anticipated structural damage. A stricter requirement for the period elongation is specified in the Eurocode 8 (CEN 2003). Eurocode 8 requires an analyst to match or exceed the target spectrum over a range of $0.2T_1$ to $2.0T_1$. At extensive levels of nonlinearity, such as performance levels of Life Safety and Collapse Prevention, the amount of period elongation is critical (Catalán *et al*. 2010). In a study by Katsanos *et al*. (2010), the required upper bound limit for spectrum matching ($2.0T_1$) is found to be excessive in most cases, due to the unlikely nature of the fundamental period of the structure doubling, unless subjected to extremely large seismic demands and structural damage. Katsanos *et al*. (2010) also proposes that the lower bound period range for which the spectral matching is conducted is taken as a function of the higher mode contributions. Rather than $0.2T_1$, that the lower period T_L is associated with the highest mode of vibration, with the effective mass corresponding to 90%.

It is noted that for single or limited range period sweep scaling approaches, the demands to systems with periods less than the fundamental mode or accounting for modes of vibration higher than the first mode can be misrepresented. Most nonstructural component systems (NCS) for example have primary modes of vibration with periods much smaller than the building itself (less than 0.2 seconds). In a survey and modal testing program of building mechanical and electrical (ME) systems, Watkins *et al*. (2009) found that more than half of the ME service equipment in typical buildings would likely be characterized as rigid (T_1<0.06 s). For these NCSs, the higher mode responses of the buildings are important. Within the period range of approximately 0.05-0.20 sec, a reasonable transfer of the vibration energy is needed to reliably predict the performance of the NCS. Scaling procedures based on the fundamental mode of a tall building can misrepresent the vibration energy associated with the NCSs, due to its lack of constraints upon the demand in the short periods. However as of yet, a consensus on the scaling for higher modes does not exist. One appealing method to account for higher mode effects and their impacts on secondary systems may be to adopt mean scaling across a period sweep, such as proposed by Somerville *et al*. (1997) and adopted by Huang *et al*. (2009). In this approach, termed the Geometric Mean Method, a motion scale factor is selected to minimize the sum of the squared errors between the design (target) spectral acceleration and spectral acceleration ordinate of the selected record over a specified period range.

In this paper, an investigation is conducted to evaluate the sensitivity of a building's nonlinear response considering four different motion scaling approaches. The scaling methods involve applying a scale factor over three different period ranges, namely: (*i*) zero to four seconds (denoted *sweep*), (*ii*) $0.2T_1$ to $1.5T_1$ (denoted *code*) and (*iii*) over the first two fundamental building periods (denoted *range*). The fourth method (*iv*) for comparison invokes scaling only at the fundamental period (T_1) of the structure (denoted *fundamental*). It is noted that the *code* (ii) and *range* (iii) methods studied herein are similar to that proposed by Hancock *et al*. (2008), whereby a scaling range of $0.5T_1$ to $2.0T_1$ is suggested. Although these and other prior studies have revealed limitations in the aforementioned scaling approaches (with particular concern rendered towards code-based scaling), herein the validity of the aforementioned scaling approaches is evaluated via comparison with spectral matching of the suite of ground motions. In this work, for reasons discussed later (Section 5.5), the spectrally matched motions are identified as the method for 'baseline' comparison to other methods. Using a suite of ground motions selected to capture magnitude and distance pairs from a probabilistic seismic hazard analysis (PSHA), each ground motion record is scaled according to the

various methods. Nonlinear time history analyses are cross-compared with each other and the baseline.

2. Building design and modeling

Three reinforced concrete special moment resisting frame (SMRF) buildings intended to represent mid and high-rise buildings are used in the study (Fig. 1). All buildings have the same assumed footprint of 45.7 m by 36.6 m. The buildings are assumed to have five bays in each direction, with building dimensions as follows: longitudinal bay width of 9.1 m, transverse bay width of 7.3 m and story height of 3.7 m. All buildings are assumed to have adequate foundation support, and therefore assumed fixed at their base. The design and analysis was conducted for the longitudinal direction of the prototype building.

For simplicity in analysis, a single bay frame was analyzed, recognizing that the frame bays provide the primary mechanism for transferring horizontal seismic demand through the building. Loads applied to the single frame bay were estimated by accounting for tributary area associated with five bays in either direction. In this context, the building behavior is idealized to that of a planar frame. Although slab and other gravity-structural components (e.g. diaphragms) as well as 3-

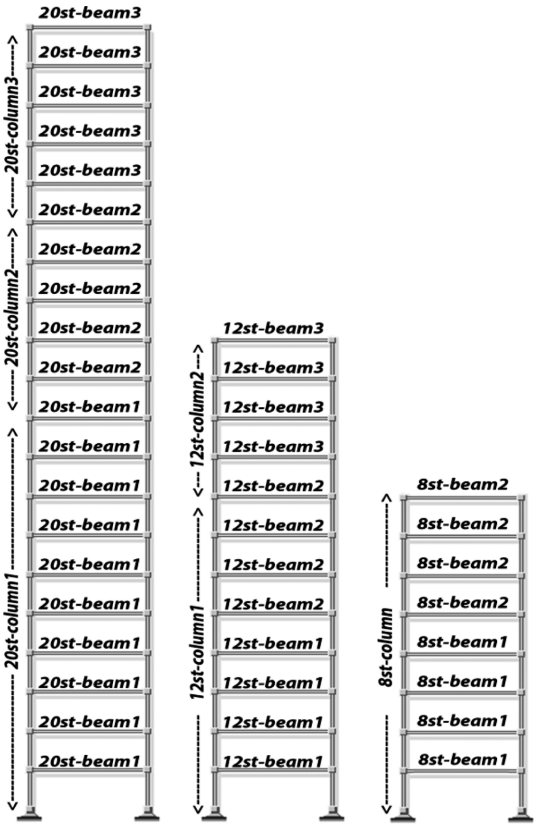

Fig. 1 SMRF building designs (Note base of model fixed and bottom of columns fixed)

dimensional behavior can influence the seismic response of a building, the planar frame simplification allows a significant reduction in the number of elements and degrees-of-freedom in the numerical model. For these models, computation time needed to perform the nonlinear time history analysis is reduced. A live load of 2.4 kN/m^2 was assumed, which is code-compliant for an office building (ICC 2006). The dead load included, in addition to the self-weight of the members, and a 25.4 cm thick two-way floor slab, a superimposed dead load of 958 N/m^2. Conventional reinforced concrete was used for the design with a 28-day unconfined compressive strength of 34.5 MPa for the beams and a range of 34.5-69.0 MPa for the columns. The weight of the concrete was assumed to be 7.2 kN/m^2. Grade 60 reinforcing steel, with a design yield tensile strength of 413.7 MPa was used throughout.

Design was governed by IBC (ICC 2006) and ACI 318-08 (ACI 2008). The IBC 2006 design code provided estimates of the base shear, period and lateral force distribution; while ACI 318-08 was utilized for the general concrete design and detailing, with particular notice to Chapter 21. In the frame designs, strong column-weak beam philosophy was adopted, i.e., the sum of the moment capacity at the columns was designed to be at least 20% greater than the sum of the moment capacity at the beams. All of the SMRF buildings designed were governed by seismic loading. In the detailing of the beams and columns, the reinforcing steel was chosen to be in one layer for simplicity and double leg #16 stirrups were selected for shear reinforcement. The confinement spacing resulted in shear reinforcement providing a minimum lateral pressure of 9% of the target f'_c (Englekirk 2003) within the assumed plastic hinge zone. Beams are assumed to be detailed symmetrically, i.e., compression reinforcement equal to the tension reinforcement. Columns are detailed with a single longitudinal reinforcement layer on each side for simplicity. Details of the building component designs are summarized in Table 1. The range of longitudinal reinforcing steel ratios ρ_l for the columns and beams is 1.1-2.7%. Additional building design details can found in Wood *et al*. (2009).

Table 1 Building component details

Element	b (cm)	h (cm)	f'_c (MPa)	Long. Reinf.	ρ_l (%)	Conf.
8st-beam1	76.2	76.2	34.5	12 - #29s	1.34	#16 @ 14.0 cm
8st-beam2	66.0	76.2	34.5	10 - #29s	1.28	#16 @ 15.2 cm
8st-column	81.3	81.3	41.4	20 - #32s	2.67	#16 @ 10.2 cm
12st-beam1	76.2	76.2	34.5	12 - #29s	1.34	#16 @ 14.0 cm
12st-beam2	71.1	76.2	34.5	11 - #29s	1.10	#16 @ 14.0 cm
12st-beam3	61.0	71.1	34.5	9 - #29s	1.28	#16 @ 15.2 cm
12st-column1	81.3	81.3	55.2	20 - #32s	2.48	#16 @ 7.6 cm
12st-column2	81.3	81.3	55.2	16 - #32s	1.98	#16 @ 7.6 cm
20st-beam1	81.3	81.3	34.5	13 - #29s	1.27	#16 @ 12.7 cm
20st-beam2	76.2	76.2	34.5	12 - #29s	1.34	#16 @ 14.0 cm
20st-beam3	61.0	71.1	34.5	9 - #29s	1.28	#16 @ 15.2 cm
20st-column1	91.4	91.4	68.9	24 - #32s	2.35	#16 @ 7.6 cm
20st-column2	86.4	86.4	68.9	20 - #32s	2.20	#16 @ 7.6 cm
20st-column3	81.3	81.3	68.9	16 - #32s	1.98	#16 @ 7.6 cm

2.1 Numerical model discretization

Numerical modeling of the prototypical planar frames idealized buildings was conducted in the OpenSees (Mazzoni 2009) platform. Two-dimensional model discretizations were developed assuming lumped masses and equivalent nodal loads. To account for large deformations, the corotational geometric transformation was invoked. Damping for the building models was set at 5% of critical, mass and stiffness proportional Rayleigh damping specified in the first two modes.

The building models were discretized using the *BeamWithHinges* element developed by Scott and Fenves (2006). This element was selected as it can be integrated with nonlinear fiber sectional discretization and has demonstrated good performance for members anticipated to undergo nonlinearity as well as softening or degradation (Scott and Fenves 2006). The *BeamWithHinges* element also eliminates the nonobjective curvature response due to its sensitivity to the number of integration points (Coleman and Spacone 2001). The element is developed as a force-based, lumped plasticity, zero-volume line element with two different sections, namely, a fiber section at each end, which represents the plastic hinge over a discrete length l_p, estimated using the Paulay and Priestley (1992) model, and an interior linear elastic section. In the development of the fiber section in the end regions, two material models are defined. Namely, the linear tension strength concrete (concrete02) and the Menegotto-Pinto model (steel02), for the reinforcing steel. The effects of confinement are accounted for using the model of Mander *et al*. (1988).

2.2 Dynamic characteristics of the building models

To determine the building dynamic characteristics, an eigenvalue analysis is carried out for all buildings models. Results from these analyses, in terms of the modal periods of vibration and modal mass participation estimates are shown in Table 2. The range of fundamental building periods is 0.89 seconds for the eight story SMRF to 2.07 seconds for the 20 story SMRF, with greater than 85% of the mass participating in the first two modes of vibration for all buildings.

3. Site location and seismic hazard

The site selected for this study is located within a densely populated region of Southern

Table 2 Building eigenvalue analysis

Building	Period (sec)			
	1st	2nd	3rd	4th
8 story	0.89	0.29	0.15	0.1
12 story	1.33	0.45	0.24	0.16
20 story	2.07	0.71	0.39	0.26
Building	Mass participation (%)			
	1st	2nd	3rd	4th
8 story	76.8	12.2	4.1	2.7
12 story	75.3	11.4	4.6	2.3
20 story	72.8	12.1	4.1	2.5

California, in the city of Charter Oaks (longitude 117.856 W and latitude 34.102 N). The site was selected due to its high rate of seismic activity and proximity to a number of known fault zones. The site class was selected as *C* (dense soil), as defined by ASCE 7-05 (2006). Using the most recently available data at the time, the National Seismic Hazard Maps (USGS 2008a), the spectral acceleration at short periods (S_s) and at a period of one second (S_1) were conservatively estimated as 2.01 g and 0.61 g, respectively, in the vicinity of the site. Using procedures of ASCE 7-05 (2006), a target design acceleration response spectrum was generated.

A PSHA of the site was used to estimate the magnitude and source-to-site distance (*M*, *R*) bins associated with a seismic hazard with a probability of exceedance of 10% in 50 years, closely corresponding to the design level scenario. The hazard analysis was conducted using the online USGS PSHA tools, with the most recent update available at the time, namely the 2002 edition of the National Seismic Hazards Mapping Project models (USGS 2008b, Fig. 2 and Table 3). The probabilistic seismic hazard analysis was conducted with respect to the peak ground acceleration due to the range of building dynamic characteristics adopted in this study (Wood *et al*. 2009).

While this negates the need for building specific record selection and may be construed as inconsistent with the motion scaling, it is noted that in practice such an approach is not uncommon due to uncertainty in actual building characteristics at a site. In this study, it was deemed more important to include a broader set of building model types. Comparison with deaggregated hazard at spectral periods near those of the taller building models indicates that hazard is under estimated in the large magnitude far field. However individual records within these bins are selected, scaled and nonlinear time history analyses conducted. These results indicate that the response results are generally within the significant statistical bounds of the PGA-based PSHA, namely that 98% of the

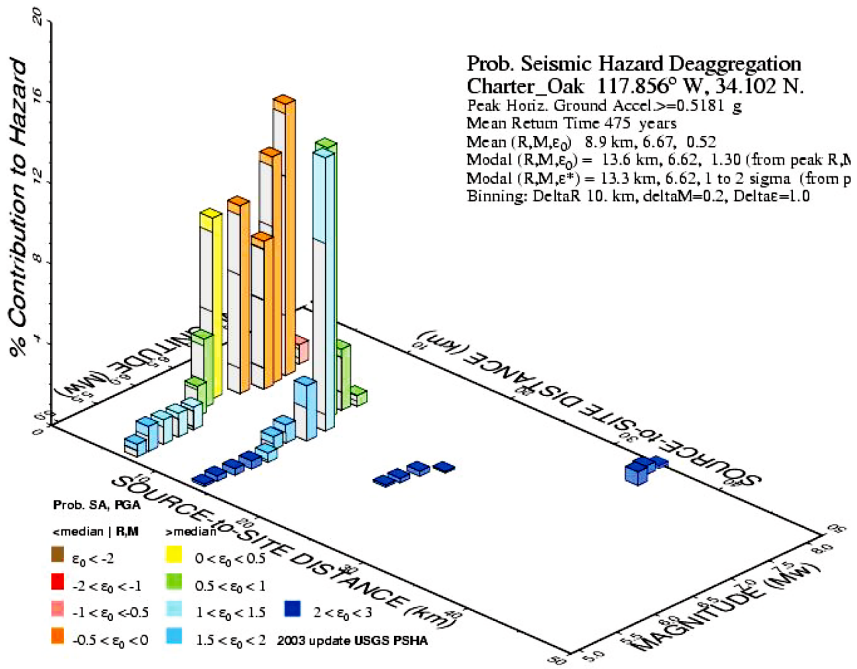

Fig. 2 Probabilistic seismic hazard deaggregation generated using the 2002 USGS interactive deaggregation tools

Table 3 Deaggregation bin details (% hazard)

M_w	Source-to-site distance (km)				
	0-10	10-20	20-30	30-40	**SUM**
5.0 - 5.25	1.9	0.4			**2.3**
5.25 - 5.50	1.2	0.3			**1.5**
5.50 - 5.75	1.2	0.4			**1.6**
5.75 - 6.00	2.6	1.1			**3.7**
6.0 - 6.25	3.4	0.9	0.1		**4.4**
6.25 - 6.50	9.0	2.7	0.2		**11.9**
6.50 - 6.75	9.3	13.6	0.3		**23.2**
6.75 - 7.00	18.6	16.4			**35.0**
7.0 - 7.25	13.5	0.5			**14.0**
7.25 - 7.50	1.0				**1.0**
7.5 - 7.75					
7.75 - 8.00				0.7	**0.7**
8.0 - 8.25				0.6	**0.6**
SUM	**61.5**	**36.4**	**0.7**	**1.3**	**99.9**

hazard is associated with sources within 20 kilometers or less, and approximately 60% of the hazard is associated with sources within 10 kilometers of the site. The deaggregation also indicates that 75% of the hazard is associated with magnitude larger than 6.50, with 58% of the hazard associated with the magnitude range of 6.5-7.0. With the 2008 deaggregation tools updated after the motions were selected, comparison between the 2002 and 2008 editions (USGS 2009) is conducted for the site of interest. This comparison indicated overall greater contributions in (M, R) (6.75-7.0, 0-10 km), (6.75-7.0, 10-20 km) and (7.0-7.25, 0-10 km) bins. A lower number of motions were selected in these bins as a result of originally used deaggregation tools.

The hazard deaggregation is used to guide the selection of ground motion records (Table 4). The selection and scaling of ground motions is a broad and currently debated topic, however, based on the recommendations of ASCE 7-05, those of Bommer and Acevedo (2004) and similarly done in Haselton's Group I (2009), it was decided that the selected ground motion records should conform to the following criteria:

• Strong motion records should be compatible with the tectonic regime anticipated at the site and of similar anticipated source mechanisms (i.e., strike-slip, reverse or normal fault),

• Magnitude-distance (M, R) pairs of the selected records should be compatible with results of the deaggregation analysis from the probabilistic seismic hazard for the site of interest. With regard to record selection, records were relaxed to magnitudes within 0.2 units of the target magnitude and 2 km of their target distance, as the dependency on seismological characteristics in site-specific record selection is not as critical when undertaking nonlinear analysis (Iervolino and Cornell 2005),

• The selected ground motion records should be compatible with the soil characteristics of the site of interest (namely site class C, with a shear wave velocity in the upper 30 meters feet ranging from 365 to 760 m/s). Records at soft soil sites were excluded,

• Ground motion records should be obtained from strong motion instruments installed in the free field.

Table 4 Selected ground motions details

	Event	Date	Location	Focal mechanism	Site class (IBC 2006)	Magnitude (M_w)
1	Baja California	Jul 2, 1987	Mexicali, Mexico	Strike-Slip	C	5.50
2	Cape Mendocino	Apr 25, 1992	Cape Mendocino, CA, USA	Reverse	C/D	7.01
3	Cape Mendocino	Apr 25, 1992	Cape Mendocino, CA, USA	Reverse	C	7.01
4	Chi Chi	Sep 25, 1999	Taichung City, Taiwan	Reverse	C	6.30
5	Friuli	Nov 12, 1999	Fruili, Italy	Reverse	C	6.50
6	Gazli	May 17, 1976	Gazli, USSR	Reverse	C	6.80
7	Irpina	Nov 23, 1980	Irpina, Italy	Normal	C	6.90
8	Kobe	Jan 16, 1995	Kobe, Japan	Strike-Slip	C	6.90
9	Kobe	Jan 16, 1995	Nishi-Akashi, Japan	Strike-Slip	C	6.90
10	Landers	Jun 28, 1992	Lucerne, CA, USA	Strike-Slip	C	7.28
11	Loma Prieta	Oct 18, 1989	San Jose, CA, USA	Reverse-Oblique	C	6.93
12	Loma Prieta	Oct 18, 1989	Saratoga, CA, USA	Reverse-Oblique	C	6.93
13	Morgan Hill	Apr 24, 1984	Morgan Hill, CA, USA	Strike-Slip	C	6.19
14	Nahanni	Dec 23, 1985	Nahanni, Canada	Reverse	C	6.76
15	Northridge	Jan 17, 1994	Castaic, CA, USA	Reverse	C	6.69
16	Northridge	Jan 17, 1994	Los Angeles, CA, USA	Reverse	C	6.69
18	San Fernando	Feb 9, 1971	Castaic, CA, USA	Reverse	C	6.61
17	San Salvador	Oct 10, 1986	San Salvador, El Salvador	Strike-Slip	C	5.80
19	Superstition	Nov 24, 1987	Superstition Mtn, CA, USA	Strike-Slip	C	6.54
20	Tabas	Jun 28, 1991	Tabas, Iran	Reverse	C	7.35
21	Victoria	Jun 9, 1980	Mexicali, Mexico	Strike-Slip	C	6.33

To obtain meaningful statistical results, a reasonable number of ground motions records are needed. Hancock *et al*. (2008) justify that 17 motions are sufficient to capture peak drift response, whereas 22 records are more suitable for capturing base rotation. Herein, a suite of 21 one directional strong motion records with the aforementioned characteristics were selected from the PEER-NGA strong motion database (PEER 2009). Of the selected motions, 11 were from the United States and Canada, two were from Italy and Japan and one each were from Taiwan, USSR (Uzbekistan), Iran, Mexico and El Salvador. The magnitudes and distance pairs of the selected ground motions represent 94% of the deaggregated contributions with ground motions of PGA>0.51 g. The details on the ground motions are summarized in Table 4 along with the spectral acceleration plots for the unscaled records in Fig. 3(a).

4. Motion scaling methods

4.1 Linear scaling

The motions are linearly scaled using four different methods. The first three methods involve scaling over a range of periods utilizing a variation of the Geometric Mean Method proposed by

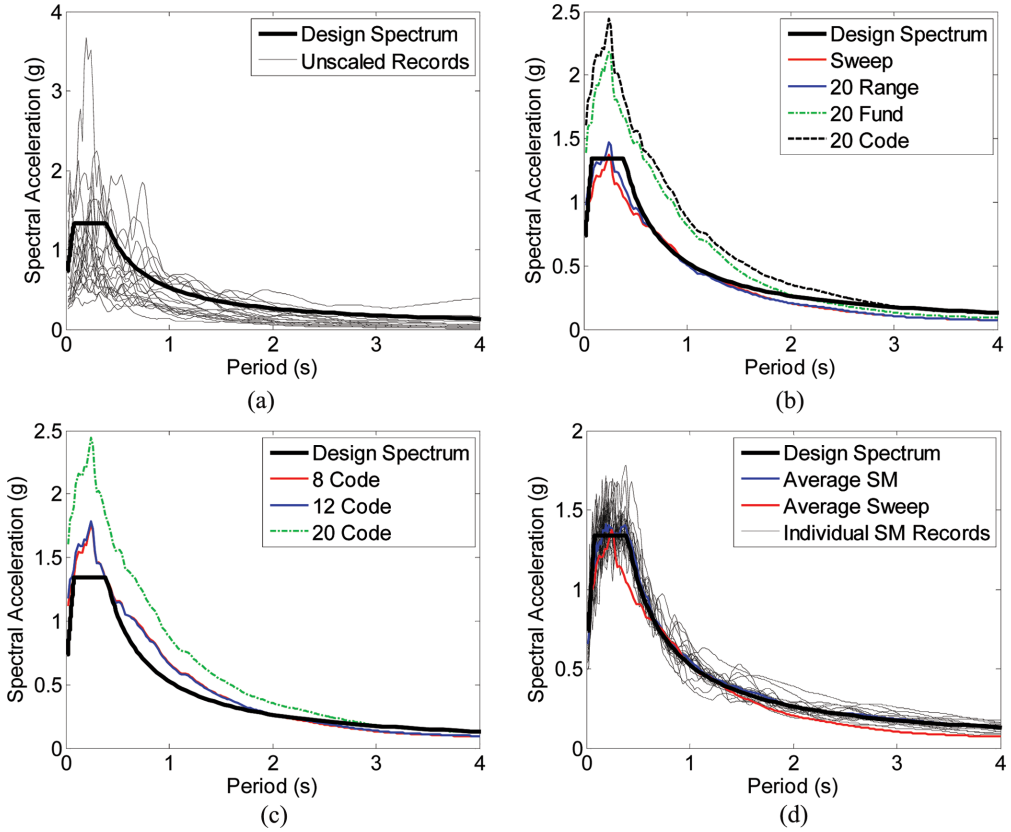

Fig. 3 Spectral acceleration curves showing: (a) the target design spectrum and unscaled motions, (b) the 20 story building against the sweep, range, fundamental and code scaling approaches, (c) the code scaling method for all buildings and (d) the average baseline (SM = spectrally matched) response with individual spectrally matched records responses. Note that the *y*-axis scale varies per subplot

Huang *et al*. (2009), which was first developed by Somerville *et al*. (1997). In this approach, the scale factor is selected to minimize the sum of the squared errors between the design (target) spectral acceleration and spectral acceleration ordinate of the selected record over a specified period range. The scale factor a for an individual record is determined as

$$a = \frac{\sum_{i=1}^{n} y_i \cdot y_i^t}{\sum_{i=1}^{n} y_i^2} \tag{1}$$

where, y_i = the spectral acceleration at period i and y_i^t = target design spectral acceleration at period i. The geometric mean scaling approach is applied in three ways: (*i*) with a period range from zero to four seconds, denoted "*sweep*" where no relevant account is made for the building dynamic characteristics, (*ii*) with a period range from $0.2T_1$ to $1.5T_1$ where T_1 represents the fundamental building mode based on the ASCE design code, denoted "*code*" and (*iii*) with a period range corresponding to the first two fundamental building modes, denoted "*range*". These various

Table 5 Scale factors for each ground motion record and summary statistics

Record No.	Sweep	Code			Range			Fundamental		
	All	20	12	8	20	12	8	20	12	8
1	0.79	1.29	0.97	1.02	0.75	0.73	0.77	1.60	0.69	0.87
2	1.36	2.00	1.53	1.61	1.09	1.12	1.31	2.01	0.94	1.19
3	1.46	2.96	2.39	2.48	1.58	2.11	2.27	1.11	1.57	1.84
4	1.89	3.04	2.22	2.27	1.57	1.67	1.94	3.20	1.62	1.27
5	1.82	3.32	2.12	2.17	2.25	1.89	1.74	4.39	2.36	2.26
6	1.03	1.85	1.28	1.36	1.05	1.35	1.07	0.97	1.14	1.47
7	2.68	3.82	3.03	3.35	1.88	2.19	2.63	2.74	2.31	1.52
8	1.17	1.70	1.32	1.37	1.17	0.97	1.00	1.44	2.09	1.45
9	0.91	2.39	1.13	1.14	1.73	1.41	0.89	1.38	2.01	2.08
10	1.82	3.90	3.13	3.15	2.22	2.33	2.65	2.09	2.51	1.99
11	2.06	3.68	2.78	2.62	2.39	2.09	2.17	5.10	2.33	2.05
12	1.23	1.71	1.37	1.55	0.83	0.99	1.43	1.15	0.75	0.89
13	1.38	2.08	1.60	1.63	1.00	1.15	1.51	2.86	1.01	0.90
14	2.37	4.59	2.99	3.08	3.99	2.82	2.28	3.75	4.10	4.59
15	0.97	1.59	1.12	1.16	0.85	0.93	0.92	1.21	0.98	0.77
16	1.57	3.26	2.44	2.11	1.92	2.09	2.15	1.35	1.67	2.18
17	1.16	1.60	1.30	1.47	0.80	0.95	1.20	0.79	0.83	0.67
18	2.27	3.79	2.79	2.82	2.22	2.11	2.20	4.74	2.88	1.95
19	0.87	1.69	1.25	1.17	1.09	0.93	1.01	2.81	1.63	0.86
20	0.55	0.99	0.74	0.67	0.57	0.56	0.59	0.56	0.86	0.59
21	1.19	1.82	1.41	1.46	1.01	1.02	1.23	2.76	0.97	0.97
Average	1.45	2.53	1.85	1.89	1.52	1.50	1.57	2.29	1.68	1.54
Standard deviation	0.57	1.04	0.77	0.78	0.80	0.64	0.64	1.35	0.87	0.89
Maximum	2.68	4.59	3.13	3.35	3.99	2.82	2.65	5.10	4.10	4.59
Minimum	0.55	0.99	0.74	0.67	0.57	0.56	0.59	0.56	0.69	0.59

methods proceed from largest period range to shortest period range considered. While the range method may appear similar to the Im_IE&2E method evaluated by Luco and Cornell (2007), it is slightly different. The Im_IE&2E method assesses the contribution of higher modes using modal combination rules (SRSS in this case), whereas the range method considered herein adopts linear scaling by calculating the equally weighted scale factor, which minimizes the error over the period range of T_1 to T_2. In the application of the code scaling approach (*ii*), an additional step is performed by increasing the scale factors by the same percentage such that the average spectra is greater or equal to the design acceleration spectrum over the specified period range of $0.2T_1$ to $1.5T_1$ to assess current code requirements. While increasing the scale factors to meet this code requirement limits the comparison to the baseline ground motion as discussed in future sections, it is performed to demonstrate the severe penalty it creates. A scaling approach considering a period range of $0.2T_1$ to $1.5T_1$ is not addressed herein, but it is anticipated that its effect would be similar to the range method while accounting for potential period elongation. The range method (*iii*) is used

to minimize the residuals over an approximate 85% mass participation range (first two fundamental modes), a similar period range suggested by Katsanos *et al*. (2010). The (*iv*) fourth scaling method involved traditionally scaling only at the fundamental period, denoted "*fundamental*". Table 5 and Fig. 3 summarize the resulting scale factors per motion considering each of the aforementioned methods and show the spectral acceleration responses.

The high spectral acceleration curves are apparent, due to the additional code prescription requiring the average spectral acceleration response be at least equal or greater to the design spectrum - this severely penalizes the scaled motions. It is interesting to observe the large difference in average spectral accelerations, particularly within the short period range apparent in Fig. 3(b), for the high-rise (20 story) building with a $T_1 = 2.07$ s. Comparing the *sweep* and *code* scaling approaches, when swept through a broader range of 0 to 4 seconds, baseline comparison with the design spectrum is more reasonable. In contrast the *code* based scaling is highly conservative (Fig. 3(c)). On average the scale factors range from about 1.5 to 2.5, with select being greater than 3.0. In the amplitude scaling of ground motions, the use of minimal scale factors are desired to minimize the bias introduced in the median nonlinear structural response, which increases with the degree of scaling to the first mode spectral acceleration (Luco and Bazzurro 2007). This issue is evaluated initially when minimizing the error over the period *sweep* range (method *i*), however this limit was relaxed to allow for the various scaling methods to be investigated. A maximum scale factor of 5.10 is obtained in the *fundamental* scaling approach for the 20 story SMRF building.

4.2 Defining baseline ground motions

For comparison with the linear scaling, a baseline is desirable. Within the context of this study, spectral matching the motion suite to develop *baseline* time histories for each event is adopted for reference comparison. To spectrally match each motion, RSPMatch (Abrahamson 1992) was used in a multiple pass approach (Al Atik and Abrahamson 2010). Each ground motion was spectrally matched using the spectral acceleration response for 5% damped of critical using four passes with increasing frequency ranges of 1-50 Hz, 0.5-50 Hz, 0.3 to 50 Hz and 0.2-50 Hz. It is noted that spectrally matching records to the design spectrum produce non-physical ground motions because this spectrum represents many potential seismic events. However, this procedure is adopted for anticipated design code demands, at the expense of nonrealistic motions lacking the troughs and valleys characteristic of the spectral acceleration. The individual spectral acceleration matched motions and the resulting average are shown in Fig. 3(d). Further analysis of the use of the spectrally matched motions as a baseline will be assessed in Section 5.6, by studying the dispersion in the nonlinear time history response parameters.

5. Nonlinear time history response results

5.1 Maximum acceleration distribution

Acceleration responses of the buildings in aggregate maximum floor level acceleration distributions are developed (Fig. 4). The maximum acceleration distribution is calculated as the average of the maximum of the absolute value acceleration at each floor level obtained from each record. Plots are shown as a function of normalized height ($h^* = h_i/H$; where h_i = height of floor i

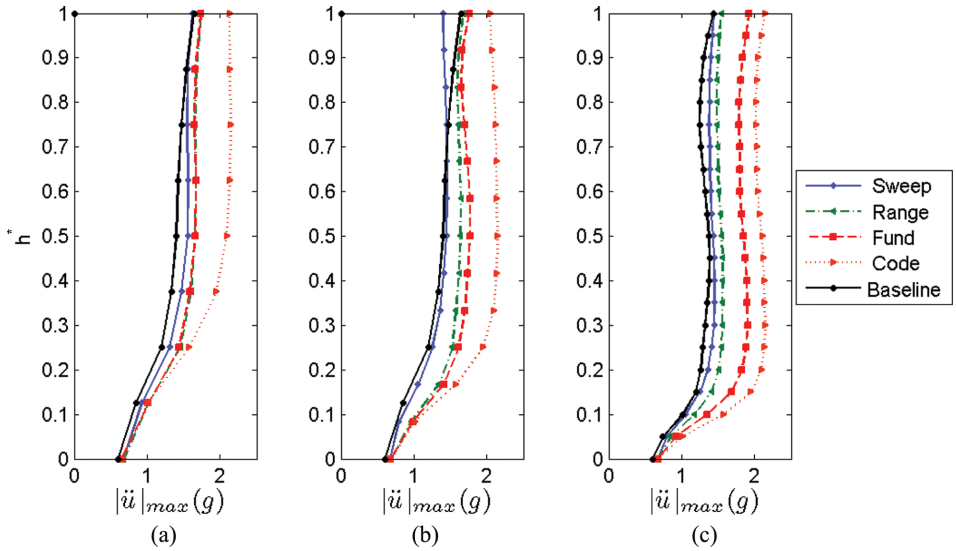

Fig. 4 Average maximum absolute floor acceleration by building type for: (a) 8 story, (b) 12 story and (c) 20 story buildings (*y*-axis unitless)

and H = overall building height) for ease in cross comparison between the different building models. At $h^* = 0$ the maximum acceleration is the average peak ground acceleration. Note that the distribution of maximum acceleration does not follow a linear trend, but rather is linear at the lower floors (shear-like mode) and parabolic (bending-like mode) at the upper floors. Such a distribution indicates higher mode effects influence the nonlinear time history response.

Considering the five different motion scaling methods, the amplitude of average maximum acceleration varied most notably in the 20 story building. For all three buildings, the *code* scaling approach provides the largest maximum acceleration distribution. The maximum acceleration experienced by all of the buildings is approximately 2 g, as result of the code prescription requiring high scaling factors so the average acceleration spectrum is above the design spectrum. In comparing the three scaling methods of: *sweep*, *range* and *fundamental*; the dispersion between the methods increases with building height, indicating that higher mode response is influenced most significantly by the motion scaling method. Note that as the buildings increase in height, the first mode participation factor decreases, increasing the influence of scaling on higher mode response. The spectrally matched (*baseline*, referred to as *BL* in subsequent discussions) method produced the lowest acceleration values, which are closest to the *sweep* method. Comparison between the four linearly scaling methods to the *BL* is discussed in more detail later.

5.2 Acceleration amplification ratio distribution

In the context of design of force-sensitive components placed within a building, it is instructive to evaluate the relation between maximum input acceleration and maximum floor acceleration. When uncorrelated, one may calculate an uncorrelated acceleration amplification ratio i.e.,

$$\Omega_i = \frac{\max(|\ddot{u}_i|)}{PGA} \tag{2}$$

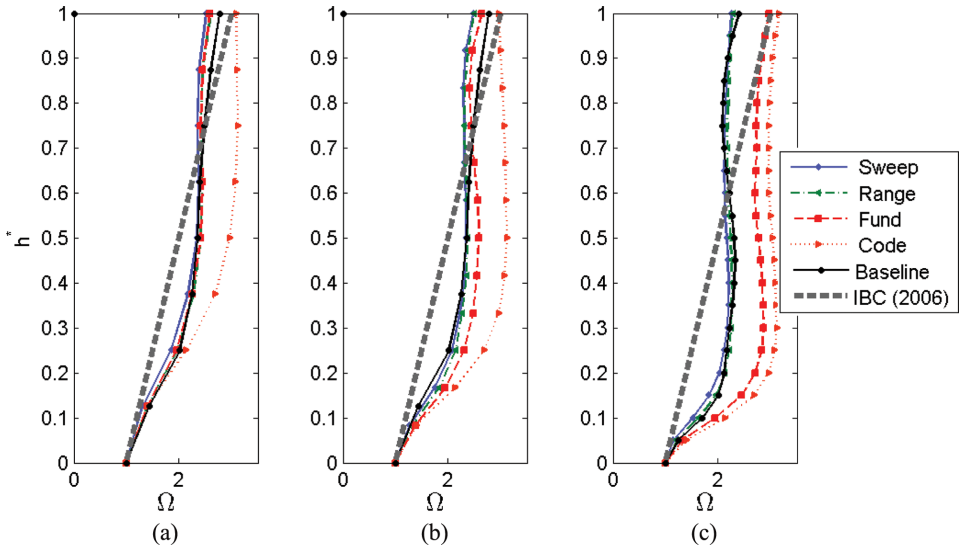

Fig. 5 Average uncorrelated acceleration amplification ratio Ω by building type for: (a) 8 story, (b) 12 story and (c) 20 story buildings (*x*- and *y*-axes unitless)

Where $\ddot{u}_i$ = the acceleration response of floor level i and PGA = the peak ground acceleration. This relationship is uncorrelated in the sense that the maximum floor level acceleration may not necessarily occur simultaneously with the peak ground acceleration. The average uncorrelated acceleration amplification ratio distributions are shown in Fig. 5, considering the average of the suite of motions. The linear code-based suggestion of ASCE 7-05 (2006) is shown for comparison.

As in the average acceleration plot; these buildings demonstrate significant influence of higher modes. As a result of higher mode effects, the prescribed code values underestimate the acceleration amplification ratio in the lower most floors for taller buildings, while conservatively overestimating amplifications in the upper most floors. This amplification trend of underestimation in the lower floors and overestimating in the upper floors holds valid for the spectrally matched motions as well. The design code severely underestimates the acceleration amplification demand when the *code* scaling approach is applied for all buildings. In addition, for the 20 story building, the *fundamental* scaling is severely underestimated, but not to the same extent of the *code* scaling approach. The scaling method adopted affects the magnitude of the response, however, it does not affect the overall shape. For the *code* scaling approach, the amplification ratio for the 8 and 12 story buildings tend to plateau at the mid-height of the buildings. The *code* scaling approach provides the largest acceleration amplification. The most consistent comparison of average uncorrelated acceleration amplification ratios with the *baseline (BL)* is observed with the *sweep* and *range* methods.

5.3 Baseline normalized acceleration distribution

To compare the four linearly scaling methods to the *baseline (BL)* response, normalized acceleration is presented. In this case, the maximum floor level acceleration for each linear scaling method is normalized by the corresponding spectrally matched (*BL*) response at each floor level on a record-to-record basis. The average of the maximum normalized values are presented in Fig. 6, considering the average of the suite of motions. With the spectrally normalized acceleration values, values less

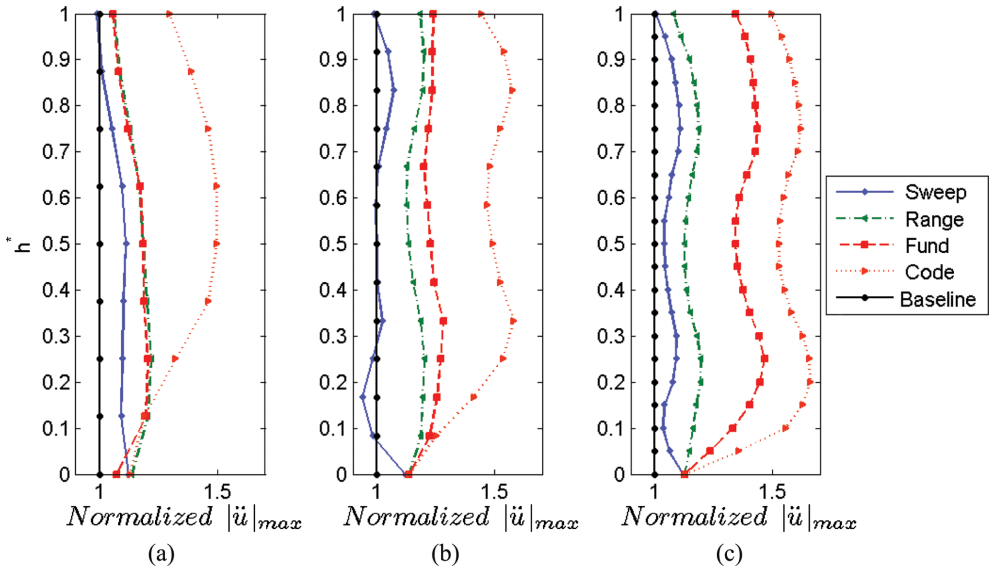

Fig. 6 Average maximum acceleration distribution normalized by the baseline response by building type for: (a) 8 story, (b) 12 story and (c) 20 story buildings (*x*- and *y*-axes unitless)

than one indicate an average response less than the *BL* and likewise average response values when values are greater than one. These results demonstrate that the *sweep* scaling method most closely matches the *baseline*, while sometimes slightly underestimating it. As may be expected, the *code* scaling method severely overestimates the maximum floor acceleration response, in excess of 166% that of the *baseline* in the twenty story building.

5.4 Baseline normalized interstory drift distribution

To compare the scaling approaches with respect to the distribution of deformation demands, the maximum interstory drift ratio per record is normalized by the *baseline (BL)* response. Similarly, the average of the maximum normalized values is presented in Fig. 7, considering the average of the suite of motions. As previously observed in the maximum acceleration distributions, the interstory distribution demonstrates higher mode effects, as the shape is parabolic in nature, and the dispersion in the results increases with increasing building height, except when comparing the *code* scaling approach. When analyzing the normalized interstory drift distribution, the *sweep* and *range* scaling method closely matches the *baseline*. However, underestimation of up to 30% is observed in the lower floors for the taller, 20 story. Consistent with the acceleration response comparisons, the *code* scaling method severely overestimates the building drift responses.

5.5 Plasticity distribution

Curvature time histories provide an indication of the extent of plasticity the buildings experience during an earthquake excitation. The extent of plasticity controls the mechanism of load transfer throughout the building; therefore it is an important indicator of seismic demand distribution. To render these results graphically, plasticity distribution diagrams are developed (Fig. 8), where by

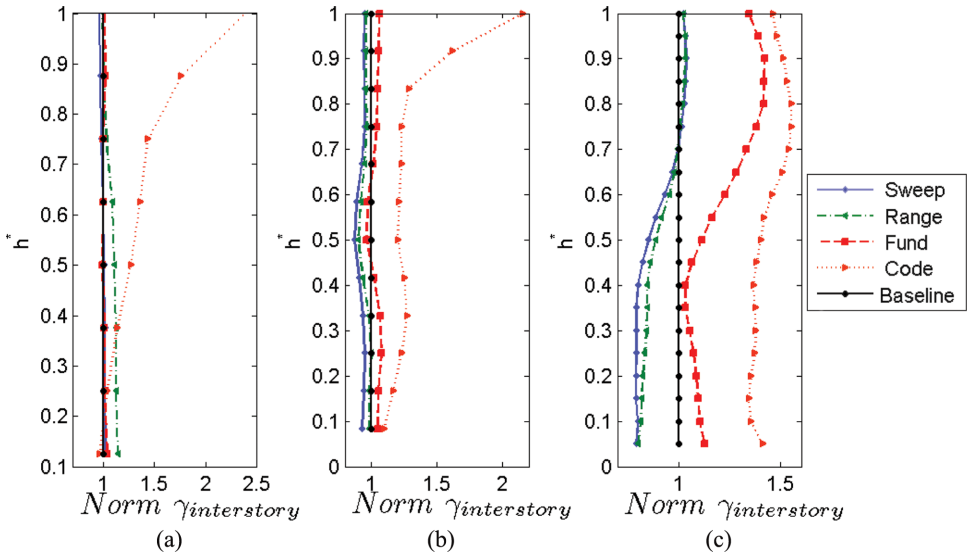

Fig. 7 Average maximum average interstory drift (γ_{is}) distributions normalized by baseline response by building type for: (a) 8 story, (b) 12 story and (c) 20 story buildings (x- and y-axes unitless)

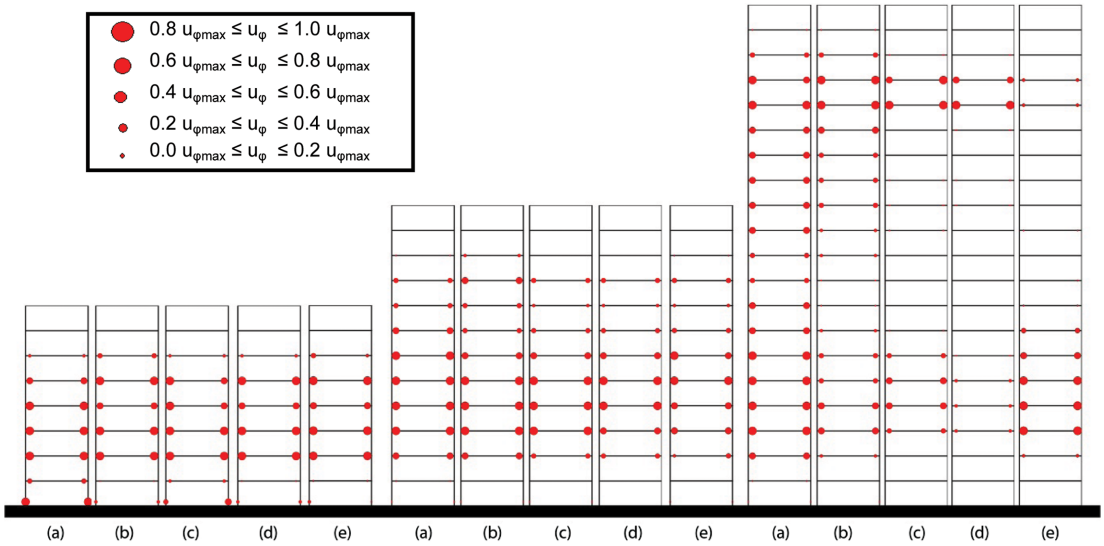

Fig. 8 Average maximum plastic rotation induced from time history analyses. From left to right: eight, twelve and twenty story buildings scaled according to the follow methods: (a) code, (b) fundamental, (c) range, (d) sweep and (e) baseline (*BL*)

average maximum curvature ductility values are reported (Table 6), considering the suite of ground motions. These plasticity distribution diagrams show a normalized bubble size at the locations where plasticity occurred and are reported as the average maximum of all ground motions. For the 8 story building, only minimal differences exist when comparing the linear scaling approaches with the *baseline (BL)*, the most significant difference being development of plastic hinging at the

Table 6 Average and normalized maximum curvature ductility (μ_ϕ) demands

Building	Scaling method	μ_ϕ	μ_ϕ^i/μ_ϕ^{BL}
8-story	Code	2.32	1.48
	Fundamental	1.55	0.99
	Range	1.84	1.17
	Sweep	1.62	1.03
	Baseline	1.57	1.00
12-story	Code	2.00	1.22
	Fundamental	1.62	0.99
	Range	1.48	0.90
	Sweep	1.44	0.88
	Baseline	1.64	1.00
20-story	Code	2.24	1.54
	Fundamental	1.99	1.37
	Range	1.25	0.86
	Sweep	1.27	0.88
	Baseline	1.45	1.00

column base of the building. However, for the 12 and 20 story buildings, more differences are observed. A concentration in upper floor plastic demands is most evident for the 20 story building, when subjected to the *sweep*-scaled motions. In contrast, the *range* scaling method results in plastic demands that are well distributed with elevation, indicating a mixture of fundamental and higher modes contributing to the response. The *fundamental* scaling method on the other hand, results in a primarily first-mode dominated plasticity distribution. The *code* scaling approach demonstrates a primarily first mode dominated plastic distribution as well, with more beam ends experiencing plastic deformations throughout the height of the building. The amount of plasticity experienced by these buildings was moderate, with average maximum curvature ductility values ranging from about 1.3 to 2.3. The *code* scaling approach resulted in the largest average maximum curvature ductility of 2.32 for the 8 story building, while the *range* scaling approach resulted in the minimum value of 1.25 for the 20 story building.

When comparing the average maximum curvature ductility demands to the *baseline (BL)* response results variations are observed per building type. For comparison, a ratio of μ_ϕ^i/μ_ϕ^{BL} is conducted by normalizing the maximum curvature ductility by the maximum curvature ductility corresponding to the *baseline*. For the eight story building, both the *fundamental* and the *sweep* method resulted in average maximum curvature ductility demands within 3% that of the *baseline*. For the 12 story building, the fundamental scaling approach resulted in average maximum curvature ductility demands within 1%, with the *range* and *sweep* methods within 10% and 12% respectively of the *baseline*. In the 20 story building analysis, the *sweep* method provided the most robust comparison with average maximum curvature ductility demands of within 12% of the *baseline*, followed closely by the *range* method, which was within 14% of the *baseline*. The *range* method also best represented the occurrences of plasticity throughout the height of the building. For the 20 story building, the *fundamental* scaling approach resulted in a poor representation of the spectrally matched plasticity demands.

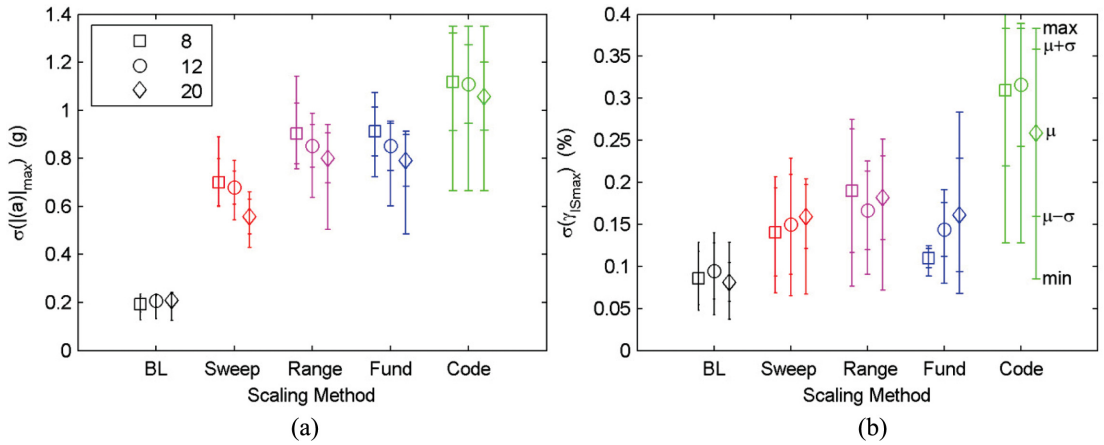

Fig. 9 Dispersion comparison of the building response (left to right: 8, 12 and 20 stories) by scaling method: (a) standard deviation of the maximum acceleration and (b) standard deviation of the interstory drift values. The middle marker (annotated as μ) identifies the average standard deviation (of all floor levels) for that particular scaling method, the inner set of error bars indicate the standard deviation of the standard deviations per floor level (annotated as $\mu \pm \sigma$) and the outer set of error bars indicate the upper and lower bound of the standard deviations (annotated as min or max, i.e., envelope) for a given scaling method

5.5 Evaluating the robustness of the spectrally matched motions as a baseline

To assess the validity of use of the spectrally matched ground motions as a baseline (assuming that they are unbiased records) for comparison to other methods investigated herein, the dispersion between scaling methods is analyzed. By comparing the standard deviation of the nonlinear response parameters (acceleration and interstory drift) for each method, it is found that the dispersion under the spectrally matched case is the smallest (Fig. 9). The spectrally matched case has the smallest average standard deviation per floor level comparison and the smallest range of standard deviations, supporting its consideration as a baseline for comparison, since record to record variability of the building response is greatly reduced. One may also note that the dispersion in the sweep method is lowest, when compared to the other scaling methods. These results were consistent with distribution and maximum, though only maximum values are shown in Fig. 9.

6. Conclusions

Four ground motion scaling methods are considered and nonlinear time history analyses of mid- and high-rise planar frame-idealized buildings are conducted systematically using the same suite of earthquake motions. This was done in an effort to shed light on the most reasonable scaling approach for use when predicting nonlinear building response. A suite of spectrally matched ground motions are adopted and denoted in as the *baseline (BL)*, with the assumption that they are unbiased. The results of the analyses use these *BL* motions to compare the four scaling methods. The baseline motions experienced the least variability of the scaling methods, providing a reduced record-to-record variable comparison to the anticipated design code requirements. One limitation is

that these baseline motions are non-physical due to limited trough and valley characteristics of the spectral acceleration.

Nonlinear response of the planar frame-idealized buildings is evaluated in terms of floor level acceleration, uncorrelated acceleration amplification ratio, interstory drift and plasticity distributions. It is consistently observed that scaling the input motions across a sweep of periods' results in a more reasonable comparison to the *baseline*, particularly when higher modes influence the buildings nonlinear demands. These results reveal a weakness in the traditional scaling approaches in the higher modes shown by divergent acceleration and interstory drift distributions, while broad period range scaling is shown to identify the higher mode response well, when compared to the spectrally compatible motions.

In the end, the most simplistic approach of scaling across a period sweep (0 to 4 seconds was adopted herein) or range of periods (T_1 to T_2) results in a very reasonable comparison of nonlinear building demands when compared with the *baseline* response results. Of these two, the period *sweep* scaling suggests the most consistent results for the building types considered in this study. Nonetheless, the *range* scaling method adopted herein, which resulted in a period range which captured 85-90% of the mass participation resulted in reasonably robust comparison, thus supporting recent suggestions that period bounds for scaling be selected based on percentage of mass participation (e.g. Katsanos *et al*. 2010). However, from a simplicity point of view, invoking a building period-independent scaling procedure is appealing and provided a very reasonable estimation of nonlinear building demands, including buildings that were influenced by higher modes.

Acknowledgements

The first author was supported through funding provided by Hilti Corporation, NSF grant number CMMI-0721399 and an NSF IGERT Award #DGE-0966375. Helpful suggestions of Professors Rob Dowell and Rolf Eligehausen and Dr. Matthew Hoehler early in the study are greatly appreciated. Opinions, findings and conclusions expressed in this paper are those of the authors, and do not necessarily reflect those of the sponsoring agencies.

References

Abrahamson, N.A. (1992), "Non-stationary spectral matching", *Seismol. Res. Lett*., **31**(1), 30-30.

Al Atik, L. and Abrahamson, N. (2010), "An improved method for nonstationary spectral matching", *Earthq. Spectra*, **26**(3), 601-617.

American Concrete Institute. (2008), "Building code requirements for structural concrete", *ACI 318-08*, Farmington Hills, MI.

ASCE 7-05. (2006), *Minimum design loads for buildings and other structures*, American Society of Civil Engineers, Reston, VA.

Bommer, J.J. and Acevedo, A.B. (2004), "The use of real earthquake accelerograms as input to dynamic analysis", *J. Earthq. Eng*., **8**(1), 43-91.

Catalán, A., Benavent-Climent, A. and Cahis, X. (2010), "Selection and scaling of earthquake records in assessment of structures in low-to-moderate seismicity zones", *Soil Dyn. Earthq. Eng*., **30**(1-2), 40-49.

Coleman, J. and Spacone, E. (2001), "Localization issues in force-based frame elements", *J. Struct. Eng.-ASCE*, **127**(11), 1257-1265.

Englekirk, R.E. (2003), *Seismic design of reinforced and precast concrete buildings*, Wiley, NJ.
European Committee for Standardization (CEN) (2003), *Eurocode designing of structures for earthquake resistance-Part 1: General rules, seismic actions*, prEN 1998-1, Final Draft.
Hancock, J., Bommer, J.J. and Stafford, P.J. (2008), "Numbers of scaled and matched accelerograms required for inelastic dynamic analyses", *Earthq. Eng. Struct. D*., **37**(14), 1585-1607.
Haselton, C.B. (2009), *Evaluation of ground motion selection and modification methods: Predicting median interstory drift response of buildings*, PEER Technical Report.
Huang, Y.N., Whittaker, A.S., Luco, N. and Hamburger, R.O. (2009), "Selection and scaling of earthquake ground motions in support of performance-based design", *J. Struct. Eng.-ASCE*, In Press.
ICC. (2006), *International building code 2006*, International Code Council, Falls Church, Va.
Iervolino, I. and Cornell, C.A. (2005), "Record selection for nonlinear seismic analysis of structures", *Earthq. Spectra*, **21**(3), 685-713.
Katsanos, E.I., Sextos, A.G. and Manolis, G.D. (2010), "Selection of earthquake ground motion records: A state-of-the-art review from a structural engineering perspective", *Soil Dyn. Earthq. Eng*., **30**(4), 157-169.
Luco, N. and Bazzurro, P. (2007), "Does amplitude scaling of ground motion records result in biased nonlinear structural drift responses?", *Earthq. Eng. Struct. D*., **36**(13), 1813-1835.
Luco, N. and Cornell, C.A. (2007), "Structure-specific scalar intensity measures for near-source and ordinary earthquake ground motions", *Earthq. Spectra*, **23**(2), 357-392.
Mander, J.B., Priestley, M.J.N. and Park, R. (1988), "Theoretical stress-strain model for confined concrete", *J. Struct. Eng.-ASCE*, **114**(8), 1804-1826.
Mazzoni, S., McKenna, F., Scott, M.H. and Fenves, G.L. (2009), *Open system for engineering simulation user-command-language manual*, version 2.0, Pacific Earthquake Engineering Research Center, University of California, Berkeley. <http://opensees.berkeley.edu/>.
Paulay, T. and Priestley, M.J.N. (1992), *Seismic design of reinforced concrete and masonry buildings*, John Wiley, and Sons Inc.
PEER-NGA (2009), *Pacific earthquake engineering research center: NGA database*, http://peer.berkeley.edu/nga/
Scott, M.H. and Fenves, G.L. (2006), "Plastic hinge integration methods for force-based beam-column elements", *J. Struct. Eng.-ASCE*, **132**(2), 244-252
Shome, N. and Cornell, C.A. (1998), "Normalization and scaling accelerograms for nonlinear structural analysis", *Proceedings of the Sixth U. S. Notional Conference on Earthquake Engineering*, CD-ROM, Seattle, WA
Somerville, P., Smith, N., Punyamurthula, S. and Sun, J. (1997), "Development of ground motion time histories for phase 2 of the FEMA/SAC steel project", *Report SAC/BC-97/04*, SAC Joint Venture, Sacramento, CA.
United States Geological Survey (USGS). (2008a), *Custom mapping and analysis tools*, USGS, Reston, Virginia, http://earthquake.usgs.gov/research/hazmaps/interactive.
United States Geological Survey (USGS). (2008b), *2002 Interactive deaggregations*, USGS, Reston, Virginia, http://eqint.cr.usgs.gov/deaggint/2002/.
United States Geological Survey (USGS). (2009), *2008 Interactive deaggregations (Beta)*, USGS, Reston, Virginia, http://eqint.cr.usgs.gov/deaggint/2008/.
Watkins, D., Chui, L., Hutchinson, T.C. and Hoehler, M.S. (2009), *Survey and characterization of floor and wall mounted mechanical and electrical equipment in buildings*, Structural Systems Research Project Report Series, SSRP 09/11, Department of Structural Engineering, University of California, San Diego, La Jolla, CA.
Wood, R.L., Hutchinson, T.C. and Hoehler, M.S. (2009), *Cyclic load and crack protocols for anchored nonstructural components and systems*, Structural Systems Research Project Report Series, SSRP 09/12, Department of Structural Engineering, University of California, San Diego, La Jolla, CA.

JL